Development of texture in poly(ethylene terephthalate) by plane-strain compression

A. Bellare, R. E. Cohen* and A. S. Argon†
Department of Chemical Engineering and †Department of Mechanical Engineering, Massachusetts Institute of Technology, Cambridge, MA 02139, USA
(Received 7 August 1992)

Morphological alterations induced by plane-strain compression of semicrystalline poly(ethylene terephthalate) (PET) at 190°C were studied using small-angle and wide-angle X-ray diffraction techniques, polarized light microscopy and differential scanning calorimetry. Based on the observations, a scheme of texture development is outlined. An initially spherulitic morphology transforms into one that comprises stacks of fragmented crystalline lamellae with lamellar normals oriented towards the flow direction. After some initial deformation by interlamellar sliding in the amorphous material (100)[001] chain slip operated throughout the remainder of the deformation. Up to a compression ratio of 2.6 the (100)[001] chain slip mechanism orients lamellar normals towards the compression axis. Further deformation caused fragmentation of the thinned-out lamellae and subsequent reorientation of lamellar normals towards the flow direction. Pole figure analysis indicated cooperative activity of the (100)[001] chain slip and (100)[010] transverse slip during the later stages of texture development. The (100)[010] transverse slip mechanism controlled the orientation of the crystal structure in a plane orthogonal to the flow direction. There was no evidence of (010)[001] chain slip during texture development. At a compression ratio of 3.3 pole figure analysis revealed the existence of a dual unit cell orientation that renders an overall orthotropic symmetry to plane-strain compressed PET.

(Keywords: PET; morphology; X-ray diffraction)

INTRODUCTION

Processing of semicrystalline polymers into film and fibre can often result in varying degrees of mechanical anisotropy. Anisotropy results from an alteration of the crystalline microstructure as a response to an imposed monotonically increasing deformation applied to the polymer during processing. Large amounts of strain can completely transform the initial randomly oriented spherulitic microstructure into a highly textured one. A multitude of competing crystalline deformation mechanisms control this transformation. Mechanisms such as crystalline slip, twinning and martensitic transformation can contribute in varying degrees to the overall plastic deformation of a semicrystalline polymer[1,2]. In addition to these intracrystalline deformation mechanisms, there can be compatible deformations between crystalline domains and the amorphous matrix[1–6].

Crystallographic deformation mechanisms in polycrystalline metals have been studied in great detail in the past[7,8]. Similar studies of texture development have been extended to the study of plastic deformation in semicrystalline polymers such as low-density polyethylene (LDPE)[1], high-density polyethylene (HDPE)[6,9,10] and nylon[11]. The evolution of deformation textures in HDPE by plane-strain compression has been studied recently by Galeski *et al.*[6]; a combination of transmission electron microscopy and X-ray diffraction techniques was particularly useful in elucidating the gradual and continuous transformation of a spherulitic morphology into one that comprised fragments of lamellae with a long period in the direction of flow in channel-die compression. In a companion study, Bartczak *et al.*[9] studied the plastic resistances of crystallographic deformation mechanisms using highly textured HDPE as approximations to macroscopic quasi-single crystals.

Previous orientation studies on poly(ethylene terephthalate) (PET) have focused on the phenomenon of strain-induced crystallization and crystallization from oriented amorphous PET[12–15]. In addition, the macroscopic phenomenological yield behaviour of oriented PET has been studied extensively[16–18]; a yield criterion for oriented PET was developed by conducting tensile and shear tests on sheets of drawn PET. In spite of this early work, however, the role of specific deformation mechanisms in the development of deformation textures in PET has remained unclear. The goals of this present investigation were to document morphological alterations induced by plane-strain compression and to interpret the observations in terms of the activity of underlying deformation mechanisms in both the amorphous and crystalline components. Plane-strain compression was employed for texture development to avoid spurious cavitation phenomena such as 'micronecking' observed by Peterlin during uniaxial drawing[19]. Among the plane-strain compression techniques, channel-die compression was favoured since with this mode of deformation relatively large samples of textured material in oriented bar form can be obtained for further deformation along certain directions to probe specific crystallographic deformation mechanisms[20].

* To whom correspondence should be addressed

0032-3861/93/071393-11

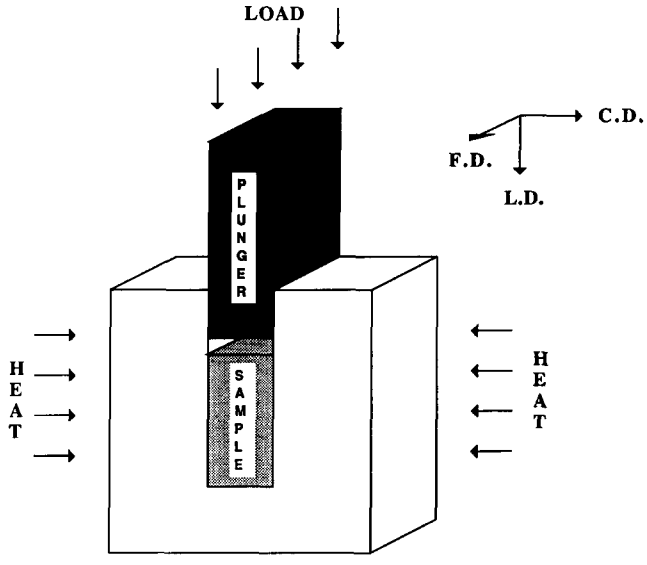

Figure 1 Schematic of channel-die compression showing the flow direction (FD), the loading direction (LD) and the constraint direction (CD)

EXPERIMENTAL

Pellets of PET manufactured by Goodyear were dried in a vacuum oven at 150°C for 48 h and compression moulded into slabs of 125 mm length, 75 mm width and 12 mm thickness. The slabs were annealed at 180°C for 1 h in a vacuum oven and subsequently machined to remove deformed outer layers. In addition, the specimens were machined to snugly fit into the channel-die of 75 mm length and 10 mm width (*Figure 1*). It was desired that all the final textured specimens should be of similar dimensions for the morphological analyses. Therefore, the initial heights of the specimens were varied depending on the desired degree of final deformation. All external surfaces of the PET specimens and the walls of the channel-die were coated with graphite powder prior to compression to minimize friction.

Plane-strain compression was performed using a channel-die previously used for other related studies on HDPE[6,9] and nylon[11]. The specimens were preheated in the channel-die to 190°C for 2 h to reach temperature equilibrium. The specimens were then compressed in a stepwise manner until the desired compression ratios were achieved. The load was released after the compressed specimens were cooled slowly to room temperature. Channel-die compressed specimens with compression ratios of 1.15, 1.8, 2.6, 3.0 and 3.3 were prepared using this procedure.

It was necessary to define a reference coordinate system with respect to specimen geometry and the external flow field. The orthogonal set of coordinates are defined as the 'loading direction' (LD) along the height of the sample along which compression is applied, 'constraint direction' (CD) parallel to the unchanging width and the 'flow direction' (FD) parallel to the length dimension undergoing extension.

Each plane-strain compressed specimen was sectioned using glass knives attached to an LKB Ultramicrotome 5. Sections of 1 μm thickness were cut perpendicular to the constraint direction and also perpendicular to the flow direction. Sectioning was performed at angles of 0°, 45° and 90° to the loading direction to evaluate any possible alteration of morphology due to the sectioning procedure. The sectioned samples were examined using polarized light at a magnification of 40 K.

A Perkin-Elmer DSC 7 was used to perform differential scanning calorimetry (d.s.c.) on cylindrical samples machined out of the plane-strain compressed samples. Cylinders of 5 mm diameter and 0.5 mm height were used. The height of the samples was parallel to the loading direction of the original specimens. Each sample was heated from room temperature to 300°C at a rate of 20°C min^{-1}. The area under the crystalline melting peak was normalized by the heat of fusion of PET crystal to obtain the degree of crystallinity. Effects of specimen shrinkage with heating were neglected.

Small-angle X-ray scattering (SAXS) experiments were performed using CuKα radiation generated from a Rigaku rotating anode X-ray source operated at 40 kV and 30 mA. A Siemens-Nicolet two-dimensional area detector with a position decoding circuit was used to observe scattered intensity that could be analysed by a dedicated computer. The detector was placed on an optical bench 1.6 m from the sample holder and an aluminium tube filled with helium was placed between the sample and detector to reduce background scattering. The incident beam was collimated using two nickel-coated mirrors. The thickness of the samples was ~0.5 mm.

Wide-angle X-ray diffraction (WAXD) was performed using another CuKα rotating anode radiation source operated at 50 kV and 60 mA. The beam from the point source was filtered using a nickel filter. A Rigaku X-ray diffractometer with a pole figure attachment was utilized. The operation of the diffractometer was controlled by a Micro VAX computer using Rigaku DMAXB software.

The diffracting planes of the triclinic crystal structure in PET were determined by performing a 2θ scan on an unoriented crystalline PET sample. The scan range was 10–55° with 2θ increments of 0.05°. The Miller indices of the crystal reflections were determined from calculations using the unit cell structure of Daubeny *et al.*[21] (*Figure 2*).

Pole figure measurements were made with rotation of the sample through the Eulerian angles α(0–90°) and β(0–360°) in steps of 5°. The pole figure intensities were normalized against the pole figure intensities of an undeformed crystallized PET standard sample and the background intensity at 2θ of 36° was subtracted from the pole figures. Pole figures were obtained in reflection and transmission modes separately. A connection angle α was carefully chosen to avoid switching of modes at areas of particular interest. The (010), (100) and ($\bar{1}$05) crystal reflections were used for pole figure analyses. The (100) and (010) planes make up two surfaces of the unit cell of PET and were chosen to simplify the analysis of lattice orientation. The reflection from the (001) plane was not observed. However, the ($\bar{1}$05) plane oriented at ~10° from the *c*-axis was used to monitor the *c*-axis orientation. This crystal reflection has been used in previous orientation studies on PET[22,23].

RESULTS

Deformation resistance

The average compression resistance plotted against compression ratio in the channel-die compression experiment shows a relatively moderate hardening rate until a

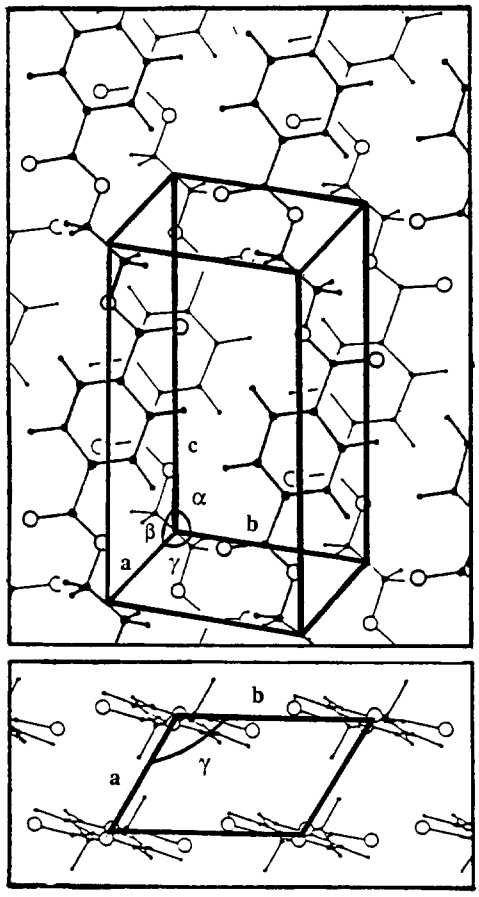

Figure 2 Unit cell structure of PET based on reference 21

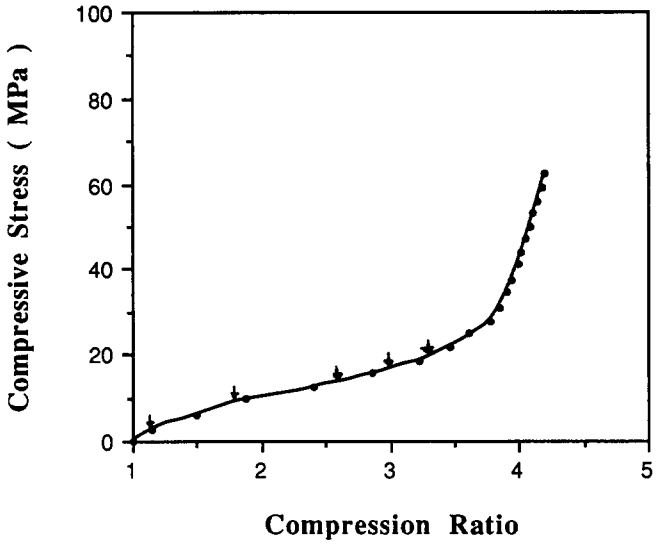

Figure 3 Compressive stress *versus* compression ratio for channel-die compression of a slab of PET at 190°C

compression ratio of 2.0 is reached, as shown in *Figure 3*. Thereafter the polymer undergoes more rapid strain hardening up to a compression ratio of 4.2, whereupon fracture occurs. The arrows indicate the various compression ratios at which the process was arrested to analyse the evolving texture due to the compression of the PET.

Analysis of the d.s.c. melting peaks indicates an initial crystallinity of ~34% followed by a gradual increase in crystallinity with compression, as shown in *Table 1*. There is no significantly large or abrupt change in crystallinity to suggest the presence of any abrupt event during texture development in plane-strain compression. However, the crystallinity increases gradually with compression ratio up to 2.6. Further deformation results in a gradual decrease in crystallinity. This latter occurrence can be explained in terms of lamellar fragmentation and the evolution of a new long period as indicated by SAXS observations; see below.

Polarized light micrographs of the semicrystalline morphology observed from the constraint and the flow directions reveal the nature of the deformation of the initial spherulitic morphology. As can be seen in *Figures 4* and *5*, the initial microstructure is spherulitic with spherulites roughly 20 μm in diameter. Significant deformation of spherulites cannot be detected by the eye up to a compression ratio of 1.8. Thereafter, monotonic spherulite elongation along the flow direction occurs. No shear banding or other inhomogeneities of deformation are found in the specimens. The boundaries of spherulites do not disappear even at high deformation ratios, although the internal structure of the spherulites is completely destroyed and a new long period emerges, as indicated by SAXS observations. However, the outlines of the initial spherulites are highly elongated along the flow direction.

Small-angle X-ray scattering

SAXS exposures were made on specimens sectioned from the compressed specimens with compression ratios of 1.15, 1.8, 2.6, 3.0 and 3.3 and viewed in the constraint, loading and the flow directions. The results are shown in *Figures 6a–e*. The SAXS pattern of the undeformed sample is an isotropic ring, indicating a random distribution of lamellae in the spherulites with an observed long period of ~8.5 nm.

The SAXS pattern of the sample compressed to a ratio of 1.15 (*Figure 6a*) is elliptical with the long axis along the loading direction. This corresponds to a decrease in long period along the loading direction. Such a decrease is expected with increasing compressive strain and a general affine behaviour. There is no significant change in the long period spacing of the SAXS maximum intensity along the flow direction. However, a slight shift in peak intensity is observed towards an angle of $\pm 45°$ from the loading direction, resulting in a diffuse four-point pattern. Corresponding WAXS pole figures, discussed below, do not indicate significant activity of slip mechanisms at a compression ratio of 1.15. Therefore, the lamellar orientation (SAXS) largely reflects interlamellar sliding, which is expected to occur due to its relatively low resistance at 190°C (the temperature at which channel-die compression was performed).

A four-point SAXS pattern viewed from the CD

Table 1 Change in crystallinity with compression ratio measured by differential scanning calorimetry

Compression ratio	Crystallinity (%)
1	34.1
1.15	34.9
1.8	36.6
2.6	39.8
3.0	37.7
3.3	35.9

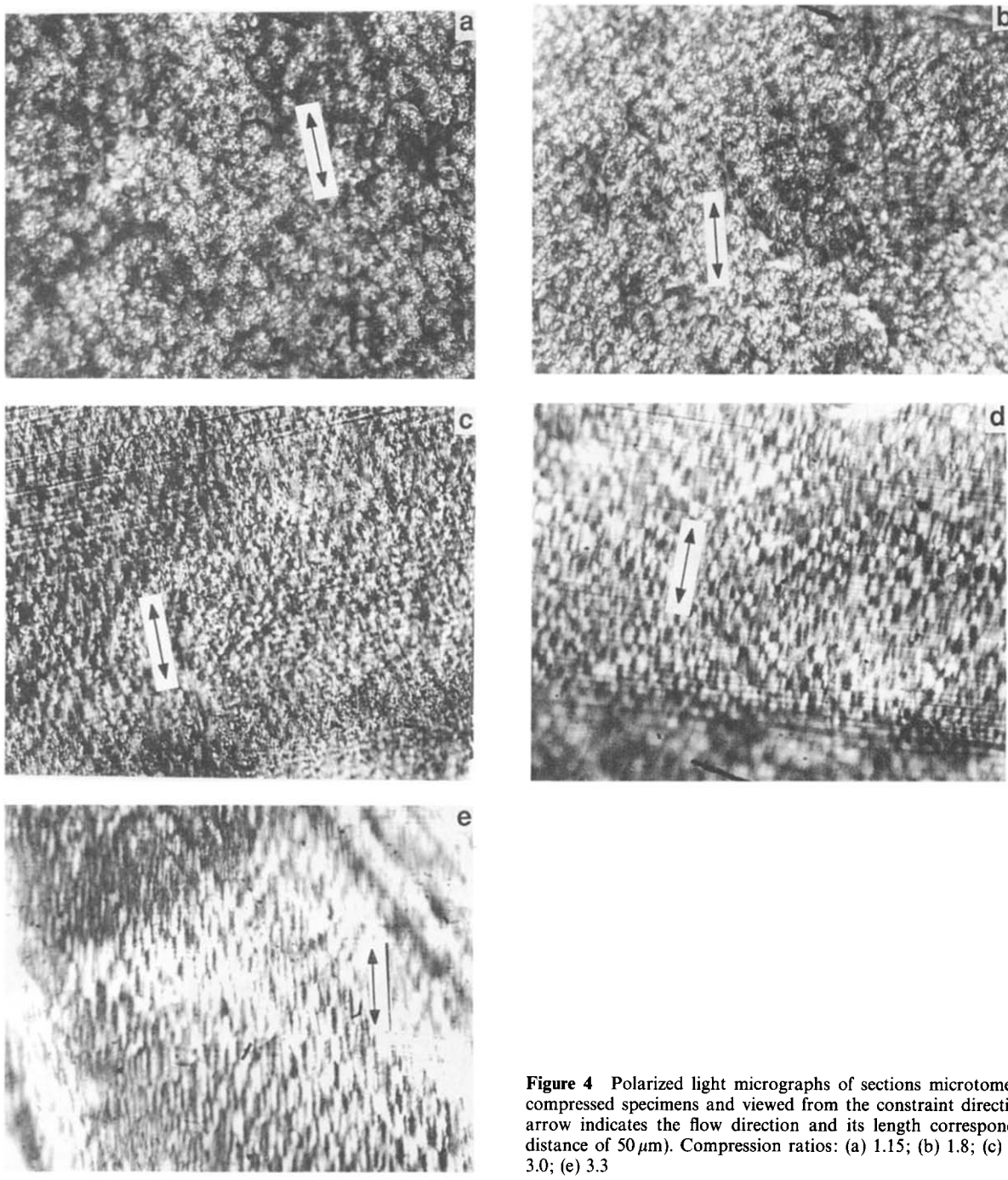

Figure 4 Polarized light micrographs of sections microtomed from compressed specimens and viewed from the constraint direction (the arrow indicates the flow direction and its length corresponds to a distance of 50 μm). Compression ratios: (a) 1.15; (b) 1.8; (c) 2.6; (d) 3.0; (e) 3.3

direction is well developed by a compression ratio of 1.8, as can be seen in *Figure 6b*. In addition there is further movement of the peaks towards the loading direction accompanied by the disappearance of intensity observed from the flow direction, indicating that the lamellae which were initially oriented with their normals in the FD direction must undergo intense kinking and shear strain. Pole figure analysis, presented below, reveals the activity of a chain slip mechanism that induces rotations of lamellae normals towards the loading direction. As will become clear from the discussion, chain slip controls the extent of shear in the lamellae and thereby the reduction in long period.

At a compression ratio of 2.6 the scattered intensity along the flow direction strengthens again, as can be seen in the SAXS patterns viewed both from the CD and LD directions in *Figure 6c*. In addition, the intensity maxima of the four-point pattern is increasingly diffuse and moves radially outwards, indicating a further decrease in long period. This is interpreted in terms of further thinning of lamellae due to chain slip. The diffuseness and reduction in intensity indicate disruption of the thinned lamellar stacks. The overall intensity of the pattern viewed along the FD direction is considerably lower, suggesting the reappearance of lamellae with normals oriented towards the FD direction (i.e. with a long period along the FD direction). The broadness of the pattern viewed from the CD direction indicates that the newly formed lamellae must have a small dimension along the loading direction relative to the length of the original lamellae of undeformed spherulites.

The four-point pattern completely transforms into a

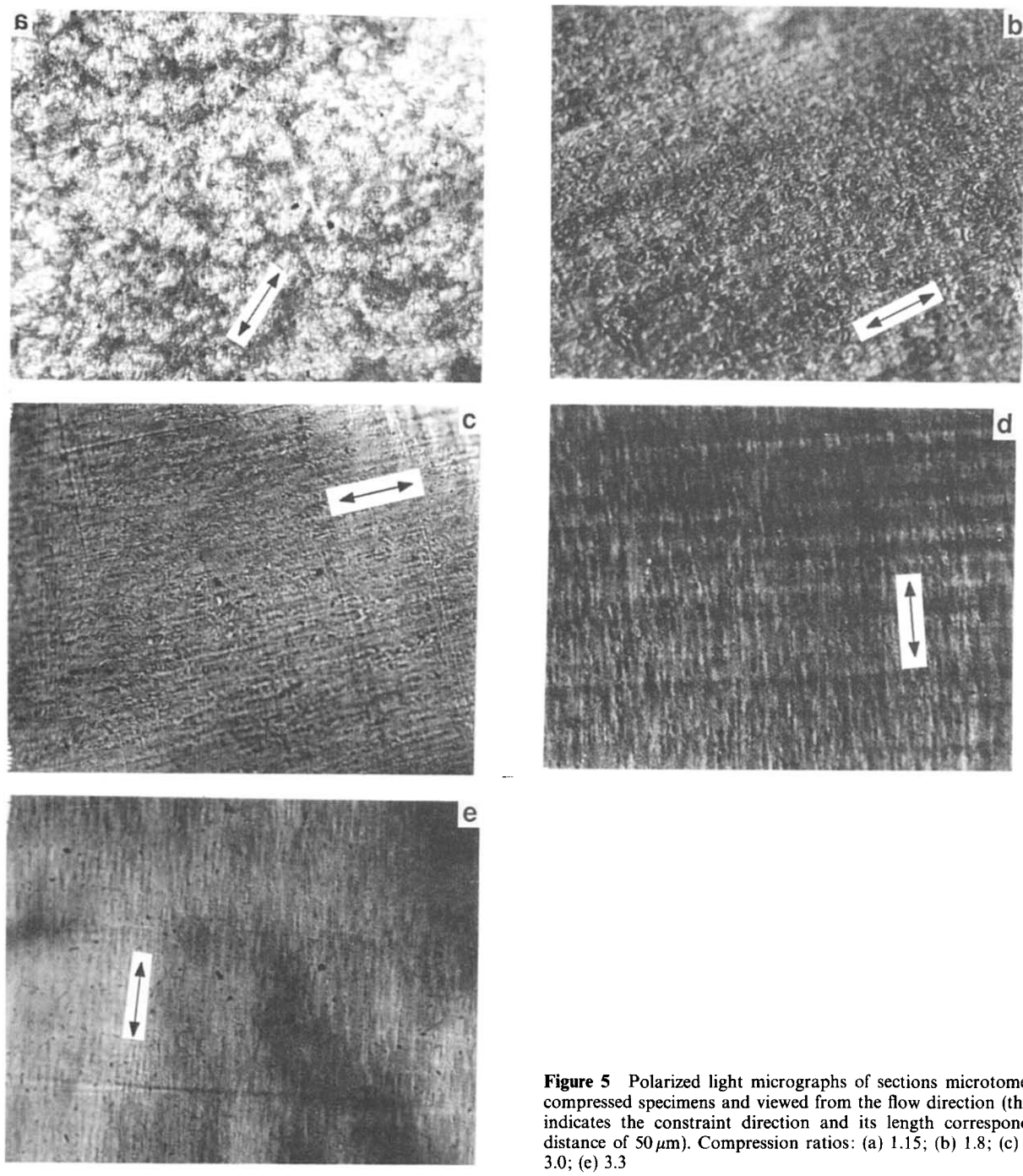

Figure 5 Polarized light micrographs of sections microtomed from compressed specimens and viewed from the flow direction (the arrow indicates the constraint direction and its length corresponds to a distance of 50 μm). Compression ratios: (a) 1.15; (b) 1.8; (c) 2.6; (d) 3.0; (e) 3.3

very broad two-point pattern by a compression ratio of 3.0, as can be seen in *Figure 6d*. The intensity of the FD direction SAXS pattern is now further reduced. This indicates that beyond a compression ratio of 2.6, fragmentation of the thinned-out lamellae and the reconstruction of a new long period occurs continuously. There is relatively less change in the SAXS patterns on further compression to 3.3 (*Figure 6e*). Taken overall, the results of SAXS show that initial deformation of the lamellae during channel-die compression consists primarily of intense lamellar shear resulting in their thinning and the rotation of lamellar normals towards the LD direction, followed by lamellar fragmentation and the emergence of a new long period along the flow direction. The crystallite fragments associated with the new long period have a much smaller dimension along the loading direction than the length of the lamellae in the spherulites.

Wide-angle X-ray diffraction

The 2θ scan of unoriented crystalline PET reveals a number of crystalline reflections, as shown in the scan of *Figure 7*. The 2θ scans of channel-die compressed PET specimens sectioned perpendicular to the LD, CD and FD directions reveal increased diffracted intensity of the (100), (010) and ($\bar{1}$05) planes in the three respective directions relative to the other crystal reflections (*Figure 8*). This indicates that these three reflections should be the most suitable for an accurate measurement of orientation of channel-die compressed PET.

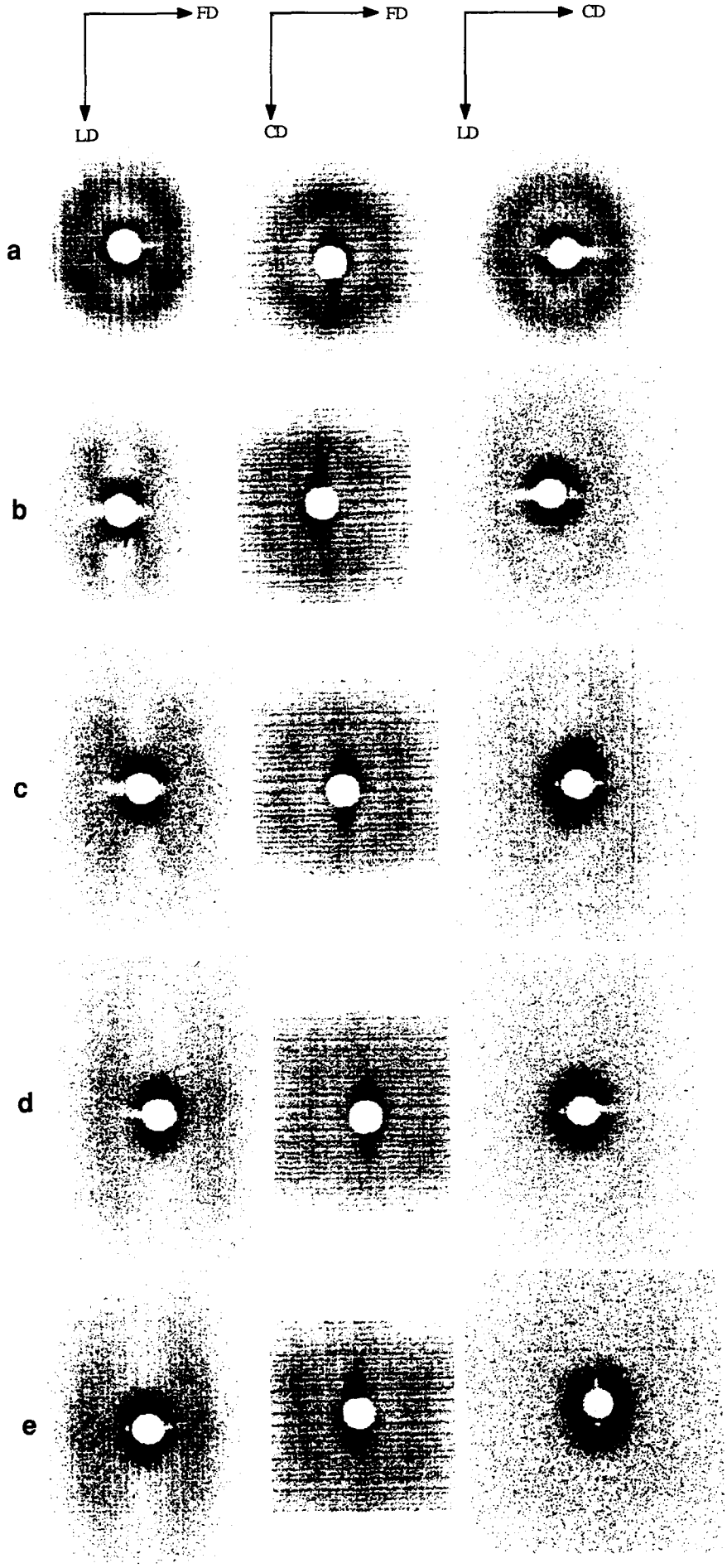

Figure 6 Small angle X-ray scattering patterns observed from the constraint (CD), loading (LD) and flow (FD) directions for samples compressed to ratios of: (a) 1.15; (b) 1.8; (c) 2.6; (d) 3.0; (e) 3.3

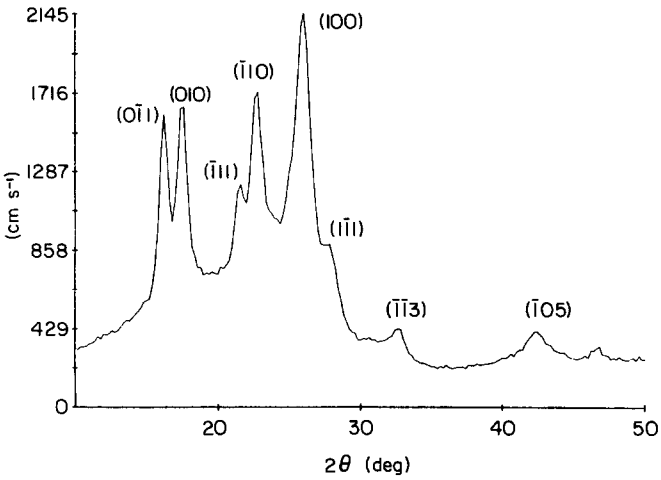

Figure 7 2θ scan of unoriented semicrystalline PET indicating Miller indices of observed crystal reflections

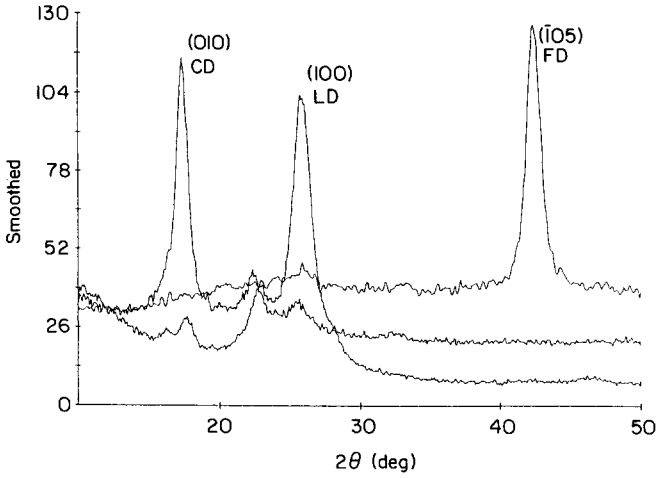

Figure 8 2θ scans of channel-die oriented PET with a compression ratio of 4.2 observed from the loading (LD), constraint (CD) and flow (FD) directions

Pole figure analysis of channel-die compressed PET

The pole figures of normals to the (100), (010) and (1̄05) planes are presented in *Figures 9–13* with the LD direction along the north–south direction and the CD direction along the equatorial direction. The changes in orientation of pole densities with compression are explained in terms of the crystallographic slip mechanisms active during the plastic deformation.

The densities in the pole figures of the sample with a compression ratio of 1.15 are not concentrated in any specific region and therefore do not indicate significant recognizable activity of any slip mechanism (*Figure 9*). However, by a compression ratio of 1.8 the high pole densities at the centre of the (1̄05) pole figure indicate clustering of chain orientation along the FD direction (*Figure 10c*). This chain orientation along the FD direction is due to the activity of the (100)[001] chain slip mechanism; also consistent with this mechanism, the (100) pole figure contains increased pole density along the loading direction. This result also supports the assertion that the plastic resistance of the (100)[001] slip is lower than that of the (010)[001] chain slip or the (100)[010] transverse slip mechanisms. From crystal symmetry conditions, the pole density distribution of the (010) pole figure must increase along arcs about the equatorial (CD) axis in the vicinity of 0° and 180°. The observations in the (010) pole figure of *Figure 10b* are consistent with this requirement.

At a compression ratio of 2.6 (*Figure 11*) the (100)[010]

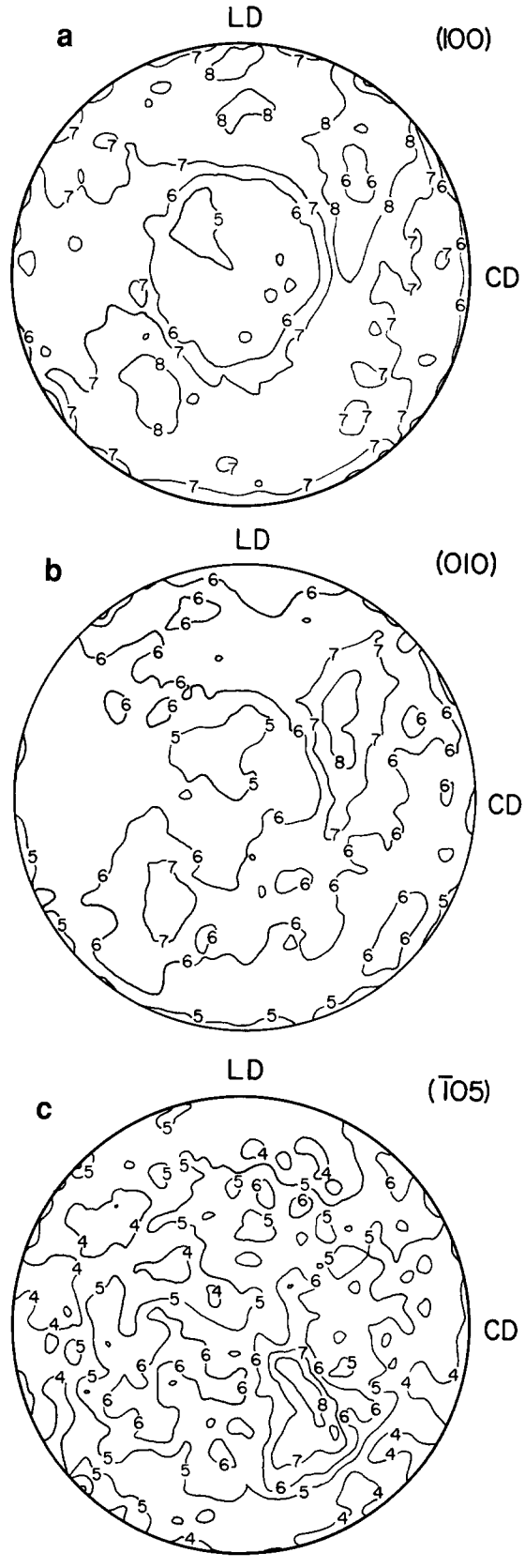

Figure 9 Pole figures for PET sample compressed to a ratio of 1.15 and corresponding to the normals of the following crystal planes: (a) (100); (b) (010); (c) (1̄05)

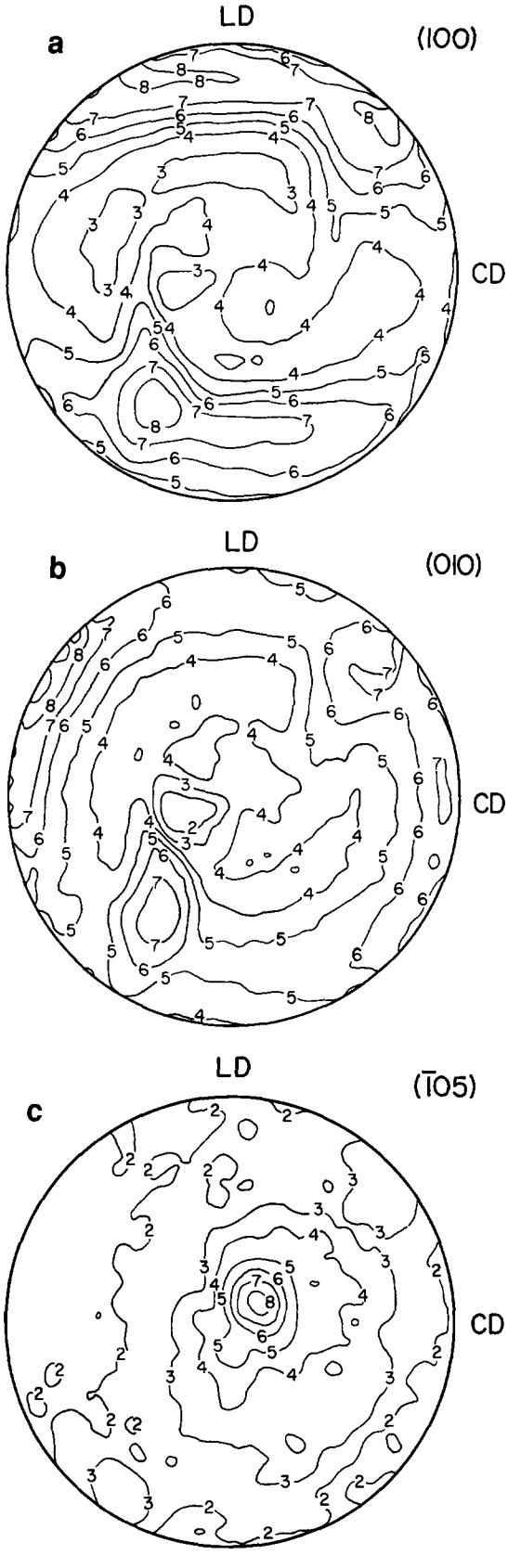

Figure 10 Pole figures for PET sample compressed to a ratio of 1.8 and corresponding to the normals of the following crystal planes: (a) (100); (b) (010); (c) (1̄05)

transverse slip preferentially orients the (100) plane normal towards the loading direction along an azimuthal path. Due to crystal symmetry conditions the pole of the (010) plane simultaneously moves towards an azimuthal angle of 22° with respect to the (CD) equator. The pole figures indicate further activity of the (100)[001] chain slip as the (1̄05) peak sharpens, i.e. there is additional chain orientation along the FD direction. Activation of the (010)[001] chain slip would have resulted in shifting of the (010) poles towards the LD direction. However,

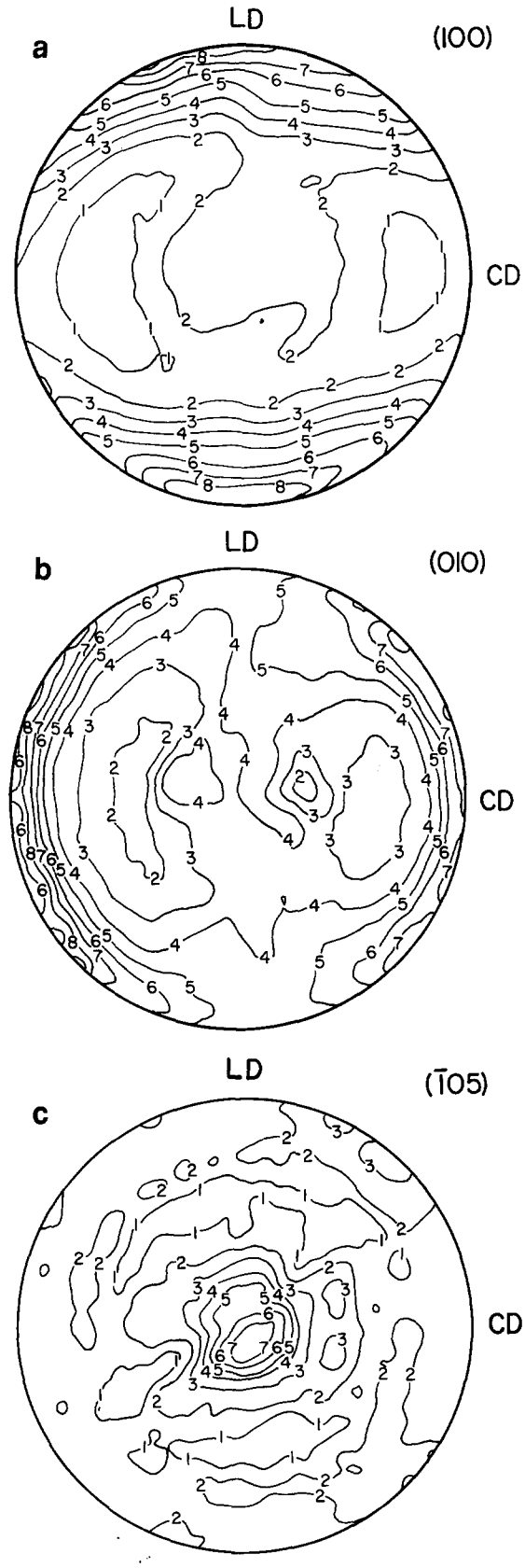

Figure 11 Pole figures for PET sample compressed to a ratio of 2.6 and corresponding to the normals of the following crystal planes: (a) (100); (b) (010); (c) (1̄05)

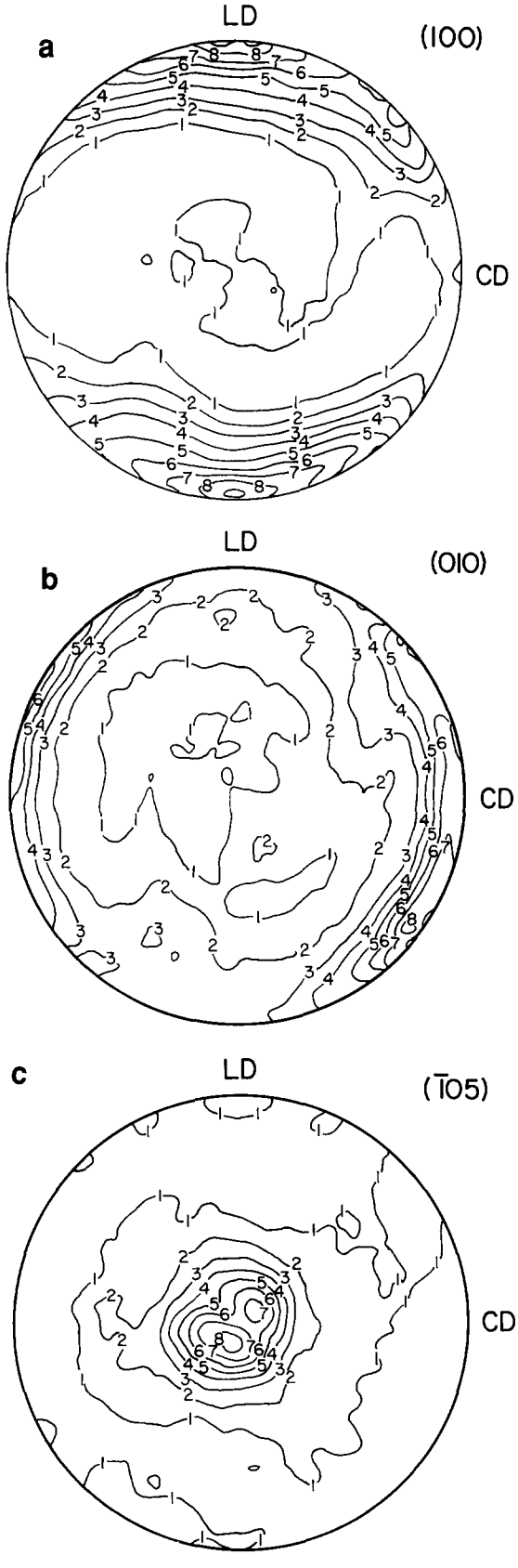

Figure 12 Pole figures for PET sample compressed to a ratio of 3.0 and corresponding to the normals of the following crystal planes: (a) (100); (b) (010); (c) (1̄05)

the (010) pole density increases along well defined arcs about the equator (CD) and its pole density in the LD direction is negligible. This indicates that the plastic resistance of the (010)[001] chain slip is higher than that of the other two mechanisms. The (010)[001] chain slip remains largely inactive.

The pole figures of *Figure 12*, obtained from specimens with a compression ratio of 3.0, reveal higher clustering of the (100) and (1̄05) poles, indicating further activity

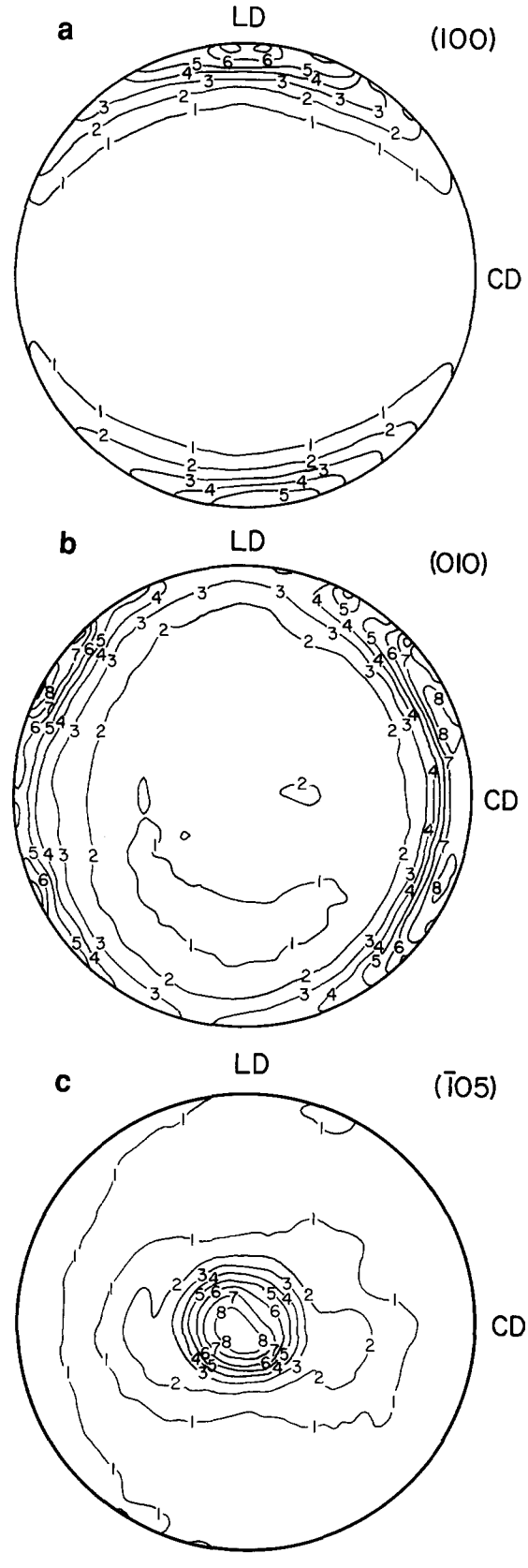

Figure 13 Pole figures for PET sample compressed to a ratio of 3.3 and corresponding to the normals of the following crystal planes: (a) (100); (b) (010); (c) (1̄05)

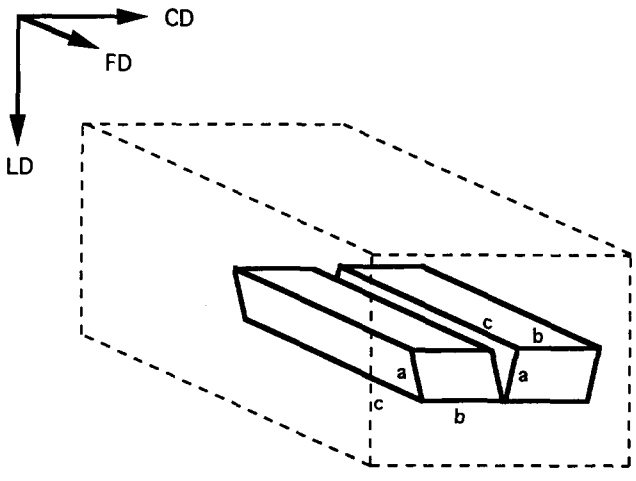

Figure 14 Schematic representation of dual orientation of the PET unit cell in a slab of channel-die textured PET

of the (100)[001] chain slip. There is a negligible change in the (010) pole figure intensities, indicating that the (010)[001] chain slip mechanism remains inactive.

At a compression ratio of 3.3 (*Figure 13*) the pole density of the (100) peak is strongly oriented along the LD direction while the ($\bar{1}05$) peak is highly oriented along the FD direction. Four pole clusters of the (010) planes are observed at an azimuthal direction of 22° about the equatorial direction. The presence of two lattice orientations with a parallel–antiparallel orientation of the unit cell in the crystalline phase are responsible for this observation, as shown in *Figure 14*. The pole figures indicate that plane-strain compressed PET possesses an orthotropic symmetry. The planes of symmetry coincide with the three planes orthogonal to the LD, CD and FD directions.

DISCUSSION

The development of texture in crystalline PET by plane-strain compression has been observed using a combination of SAXS, WAXD, polarized light microscopy and d.s.c. The set of observations can be explained in terms of the competing crystalline- and amorphous-phase deformation mechanisms. A combination of WAXD and SAXS was utilized to identify the underlying deformation mechanisms and their role in altering an initially spherulitic morphology.

Interlamellar sliding of the amorphous phase was the first observable deformation mechanism at compression ratios up to 1.15. The decrease in long period during the early stages of deformation was due to the activity of this deformation mechanism. The temperature of channel-die compression was 190°C, which is well above the glass transition temperature of PET. Therefore the deformation resistance of the amorphous regions was considerably reduced, resulting in the activation of interlamellar sliding prior to crystalline-phase deformation mechanisms, and a generally rubber-like behaviour of the samples.

The (100)[001] chain slip was the first observed crystalline deformation mechanism and must therefore have the lowest plastic resistance among the crystalline-phase deformation mechanisms. Slip resistance measurements of the (100)[001] mechanism made in a parallel study[20] revealed a critical resolved shear stress of about 38 MPa. This mechanism must have been activated after interlamellar sliding was complete and the amorphous material was locked in an extended state. The (100)[010] transverse slip was also observed, but to a lesser extent and only during the later stages of deformation. There was no evidence of (010)[001] chain slip during texture development. This slip mechanism must therefore have the highest plastic resistance of the three slip mechanisms under study. It is possible that (010)[001] chain slip was activated, but its effects were dominated by the other mechanisms.

The (100)[001] chain slip mechanism operated continuously above a compression ratio of 1.15 and was observed up to compression ratios of 3.3. Its effect on altering morphology was most pronounced at the early stages of deformation with decreased influence during the strain hardening stage (*Figure 3*) of the deformation. The (100)[001] chain slip mechanism controlled the orientation of the lamellae of the initial spherulites and continued to promote chain orientation in the lamellae associated with the new long period which appears near a compression ratio of 2.6.

The (100)[010] transverse slip mechanism controlled the orientation of the crystalline lattice in a plane orthogonal to the FD direction. There was some evidence for the activity of this mechanism by a compression ratio of 2.6, and its activity increased at higher compression ratios. This mechanism was responsible for the eventual perfection of the orientation texture during the strain hardening stages of deformation.

Deformation at the lamellar level can also be explained in terms of the deformation mechanisms discussed above. Initially, lamellar rotations occurred due to interlamellar sliding. Thereafter, the (100)[001] chain slip mechanism sheared the crystalline lamellae continuously, resulting in both thinning of the lamellae and rotation of lamellar normals towards the LD direction. Similar observations were made by Galeski *et al.*[6] on plane-strain compressed HDPE. In companion studies by Azhi and co-workers[24,25], a computer model was developed to predict lamellar orientations at various stages of plane-strain compression; results of that modelling study of HDPE showed continuous rotations of lamellar normals towards LD along with a monotonic decrease in lamellar thickness. Our experiments on PET are consistent with the general predictions of Azhi's model up to a compression ratio of 2.6, at which point further deformation resulted in a continuous disruption of the original lamellar morphology and emergence of a new long period along the flow direction of the channel-die.

The formation of a similar new long period has recently been observed[6,26] during channel-die compression of HDPE. A combination of transmission electron microscopy and SAXS elucidated deformation at the lamellar level. Widespread lamellar fragmentation was observed with lamellar rotations opposite to that observed during fine chain slip. Based on these observations, a mechanism of the transformation of the crystalline morphology was proposed: continued thinning of lamellae leads to instability, resulting in pinching off at sites of inhomogeneities and thickness irregularities in the thinned lamellae. A mechanism of topological reordering was proposed, which leads to crystallite orientation such that lamellar normals align approximately parallel to the FD direction[6]. The SAXS observations on PET are consistent with this proposed scheme of texture development by

plane-strain compression. The transformation of the four-point pattern into a two-point pattern is explained by lamellar fragmentation and subsequent reorientation. This fragmentation of thinned-out lamellae in PET begins at compression ratios of 2.6 and continues with further deformation. This fragmentation mechanism also helps to explain the gradual decrease in crystallinity above compression ratios of 2.6.

The resistances of the active deformation mechanisms have been measured in a separate study[20]. These parameters provide input into the detailed computer model developed by Azhi and co-workers[24,25] that could be adapted to predict texture development in PET.

ACKNOWLEDGEMENTS

This research has been supported by the DARPA/ONR URI programme under contract no. N00014-86-K-0768. The authors are grateful to Dr L. Lin for his assistance in the plane-strain compression experiments.

REFERENCES

1 Young, R. J., Bowden, P. B., Ritchie, J. and Rider, J. G. *J. Mater. Sci.* 1973, **8**, 23
2 Bowden, P. B. and Young, R. J. *J. Mater. Sci.* 1974, **9**, 2034
3 Keller, A. and Pope, D. P. *J. Mater. Sci.* 1971, **6**, 453
4 Pope, D. P. and Keller, A. *J. Polym. Sci., Polym. Phys. Edn* 1975, **13**, 533
5 Hay, I. L. and Keller, A. *J. Mater. Sci.* 1967, **2**, 538
6 Galeski, A., Bartczak, Z., Argon, A. S. and Cohen, R. E. *Macromolecules* 1992, **25**, 5705
7 Pierce, D., Asaro, R. J. and Needleman, A. *Acta Metall.* 1983, **31**, 1951
8 Kocks, U. F. and Chandra, H. *Acta Metall.* 1982, **30**, 695
9 Bartczak, Z., Argon, A. S. and Cohen, R. E. *Macromolecules* 1992, **25**, 5036
10 Bartczak, Z., Cohen, R. E. and Argon, A. S. *Macromolecules* 1992, **25**, 4692
11 Galeski, A., Argon, A. S. and Cohen, R. E. *Macromolecules* 1991, **24**, 3953
12 Fischer, E. W. and Fakirov, S. *J. Mater. Sci.* 1976, **11**, 1041
13 Yeh, G. S. Y. and Geil, P. H. *J. Macromol. Sci. (Phys.)* 1967, **B1**(2), 251
14 Asano, T. and Seto, T. *Polym. J.* 1973, **5**(1), 72
15 Misra, A. and Stein, R. S. *J. Polym. Sci., Polym. Phys. Edn* 1979, **17**, 235
16 Brown, N. and Ward, I. M. *Phil. Mag.* 1968, **17**, 961
17 Brown, N. and Ward, I. M. *J. Polym. Sci.* 1968, **6**, 607
18 Brown, N., Duckett, R. A. and Ward, I. M. *Phil. Mag.* 1968, **18**, 483
19 Peterlin, A. *J. Mater. Sci.* 1971, **6**, 490
20 Bellare, A. PhD Thesis, Massachusetts Institute of Technology, 1991
21 Daubeny, R. de P., Bunn, C. W. and Brown, C. J. *Proc. R. Soc. London* 1954, **A226**, 531
22 Dumbleton, J. H. and Bowles, B. B. *J. Polym. Sci., Part A-2* 1966, **4**, 951
23 Thistlethwaite, T., Jakeways, R. and Ward, I. M. *Polymer* 1988, **29**, 61
24 Azhi, S., Parks, D. M. and Argon, A. S. *ASME Comp. Mod. Sim. Mater. Proc.* 1990, **20**, 287
25 Parks, D. M. and Azhi, S. *J. Mech. Phys. Solids* 1990, **38**, 701
26 Song, H. H., Argon, A. S. and Cohen, R. E. *Macromolecules* 1990, **23**, 870